Mechanics of membrane internalization against osmotic pressure: boundary conditions make a difference

Rui Ma[1, 2, *] and Julien Berro[1, 2, 3, †]

[1] *Department of Molecular Biophysics and Biochemistry, Yale University, New Haven, CT 06520, USA*
[2] *Nanobiology Institute, Yale University, West Haven, CT 06516, USA*
[3] *Department of Cell Biology, Yale University School of Medicine, New Haven, CT 06520, USA*

(Dated: February 18, 2019)

In this paper, we study membrane deformations powered by a point force under the condition of high pressure and low tension, which is rarely studied but directly relevant for endocytosis in yeast cells with a cell wall. We show that the force-height relationship of membrane deformations under this condition is drastically different from that under conditions of high tension and low pressure. Depending on boundary conditions at the attachment point of membrane with the cell wall, the force-height relationship can exhibit qualitatively different behavior. Our theory is in excellent agreement with experimental shapes of membrane during endocytosis in yeast cells.

Clathrin-mediated endocytosis (CME) is an active process for eukaryotic cells to transport material from outside of the cell to inside [1, 2]. During CME, a patch of plasma membrane is bent into the cell and severed to release a vesicle. Deforming membrane towards the cytoplasm is opposed by membrane's resistance to bending and membrane tension. In walled cells, the inward deformation is also opposed by the high osmotic pressure [3]. For instance in yeast, the inner pressure relative to the outside of the plasma membrane can be up to $1 - 1.5$MPa [4, 5]. It is believed that as a consequence of this high pressure, the membrane invagination exhibits a narrow tubular shape in yeast with a diameter of ~ 30nm [6], while in mammalian cells the diameter is of ~ 100nm due to a relatively low pressure [7].

In the past decade several theoretical models have been proposed to account for the membrane shape evolution during CME [8–11]. Most of these models have assumed a small osmotic pressure (< 1kPa) and focused on the role of membrane tension. Such tension-dominant membrane deformations have been extensively studied in *in vitro* experiments where a membrane tether is pulled from a giant liposome [12–14]. In contrast, the pressure-dominant regime of membrane deformations, which is relevant to endocytosis in walled cells, has been rarely studied. The typical force barrier to invaginate a membrane against a membrane tension of 0.01pN/nm is only $10 - 100$pN, whereas a substantial force (~ 3000pN) is required to overcome a pressure difference of 1MPa [2, 15].

The cytoskeleton protein actin is essential for generating the forces required for CME in yeast. How actin machineries produce force to bend the membrane remains unclear. A hypothesis is that polymerization of actin filaments is converted to a pulling force acting around the tip of the invagination through a push-pull mechanism [16–19].

In addition to the force generated by actin polymerization, membrane can also be bent by proteins that induce curvature. Clathrin molecules can assemble into a cage-like icosahedral lattice composed of hexagons and pentagons [20, 21]. This structure is proposed to act as a scaffold imposing a spherical cap onto the membrane and facilitate membrane invaginations. However a recent theoretical work argues that the induced curvature of membrane cannot spontaneously lift the membrane up against high pressure. Furthermore, the induced curvature hinders CME by increasing the force needed to lift the membrane off the cell wall [10].

In this paper, we study the shape and force requirement for membrane deformations that are driven by a point force and by proteins that induce membrane curvature under conditions of high pressure and low tension. We show that the force-height (f-L) curves of pressure-dominant membrane deformations are drastically different from that of the well-studied tension-dominant case. Depending on boundary conditions, the f-L curves demonstrate qualitatively different behavior.

We consider an axisymmetric membrane patch that is attached to the cell wall on a circular base of radius R_b (Fig. 1a and b). The membrane patch is lifted up by a point force f to a height L relative to the cell wall. Outside of the circular region there is a lipid reservoir such that the membrane tension σ is kept constant, but not the area A of the membrane patch. An isotropic pressure p is exerted on the membrane, which possesses a bending rigidity κ and spontaneous curvature c_0 due to protein coating. The free energy of the membrane patch (combined with protein) can be written as

$$F = \frac{\kappa}{2}\int (2H - c_0)^2 \,\mathrm{d}A + \sigma A + pV - fL, \qquad (1)$$

where H denotes the mean curvature of the membrane [22], and V denotes the volume between the lifted membrane and the cell wall.

The surface coordinates $[R(s), Z(s)]$ of membrane are parameterized with the arclength s along the contour. They are related to the angle $\psi(s)$ via

$$\dot{R} = \cos\psi, \qquad \dot{Z} = -\sin\psi. \qquad (2)$$

Hereafter the dot indicates derivative with respect to s.

Imagine a cut at $Z = Z_0$ that divides the membrane into an upper half $Z > Z_0$ and a lower half $Z < Z_0$, the stress tensor γ_t and γ_n are the force per unit length exerted by the lower half on the upper half [23], with the tangential component

$$\gamma_t = \sigma + \frac{1}{2}\kappa\left[\left(\frac{\sin\psi}{R} - c_0\right)^2 - \dot{\psi}^2\right], \tag{3}$$

and the normal component

$$\gamma_n = \kappa\frac{d}{ds}\left(\frac{\sin\psi}{R} + \dot{\psi}\right). \tag{4}$$

The shape equation derived through variational method of the free energy (1) is simply the force balance equation for the upper half along the z-axis

$$2\pi R(-\gamma_t \sin\psi + \gamma_n \cos\psi) - \pi R^2 p + f = 0. \tag{5}$$

At the attachment point $R = R_\mathrm{b}$, we impose a free hinge boundary condition (free-HBC, Fig. 1a) such that the torque tensor (torque per unit length applied by the lower half on the upper half) vanishes,

$$\tau \equiv \kappa\left(\frac{\sin\psi}{R} + \dot{\psi} - c_0\right) = 0, \tag{6}$$

or a fixed-hinge boundary condition (fixed-HBC, Fig. 1b), which requires the angle

$$\psi = 0. \tag{7}$$

At the membrane tip $s = 0$, we impose $\psi = 0$.

To demonstrate the mechanical difference between pressure-dominant membrane deformation and tension-dominant one, we calculate the characteristic tube radius R_p and force f_p set by pressure, and R_σ and f_σ set by membrane tension respectively. In the pressure-dominant case, they read:

$$R_\mathrm{p} = \left(\frac{\kappa}{2p}\right)^{1/3}, \quad f_\mathrm{p} = 3\pi R_\mathrm{p}^2 p. \tag{8}$$

In the tension-dominant case, they are [24]:

$$R_\sigma = \sqrt{\frac{\kappa}{2\sigma}}, \quad f_\sigma = 4\pi R_\sigma \sigma. \tag{9}$$

As for endocytosis in yeast cells, $\sigma \approx 0.01$pN/nm [11], $p \approx 1$MPa [4, 5] and $\kappa \approx 300 k_\mathrm{B}T$ [25]. These lead to an estimation of $R_\mathrm{p} \approx 8.5$nm and $f_\mathrm{p} \approx 700$pN. Compared with $R_\sigma \approx 250$nm and $f_\sigma \approx 30$pN, the pressure is apparently dominant over membrane tension as the major factor that opposes endocytosis. For the rest of the paper, we will focus on the regime where $f_\mathrm{p} \gg f_\sigma$.

We first study membranes without spontaneous curvature, i.e., $c_0 = 0$. Eqs. (2) and (5) are solved with a shooting method for various base radii R_b [26]. For both boundary conditions, the f-L curve is non-monotonic and a force peak F_max appears at a relatively small height L when the membrane is dome-shaped (Fig. 1c and d, inset). As the membrane is lifted further up, the morphology goes from a dome-shape to an Ω-shape, which is indicated by the appearance of a narrow neck. The force f then drops down with L and approaches the elongation force $F_\mathrm{e} \equiv \lim_{L\to\infty} f(L)$, which equals f_p in this case. This trend is similar to the f-L curve for tension-dominant deformation [24]. However, two striking differences should be noted: (i) In the pressure-dominant regime discussed here, a nonzero initiation force $F_\mathrm{init} \equiv f(L = 0)$ is needed to lift the membrane patch just off the cell wall and F_init scales with the base radius R_b as $F_\mathrm{init} = \frac{3}{8}\pi R_\mathrm{b}^2 p$ for free-HBC and $F_\mathrm{init} = \frac{1}{4}\pi R_\mathrm{b}^2 p$ for fixed-HBC [26](Fig. 1e and f, solid lines and diamonds), whereas in the tension-dominant regime, $F_\mathrm{init} = 0$ is

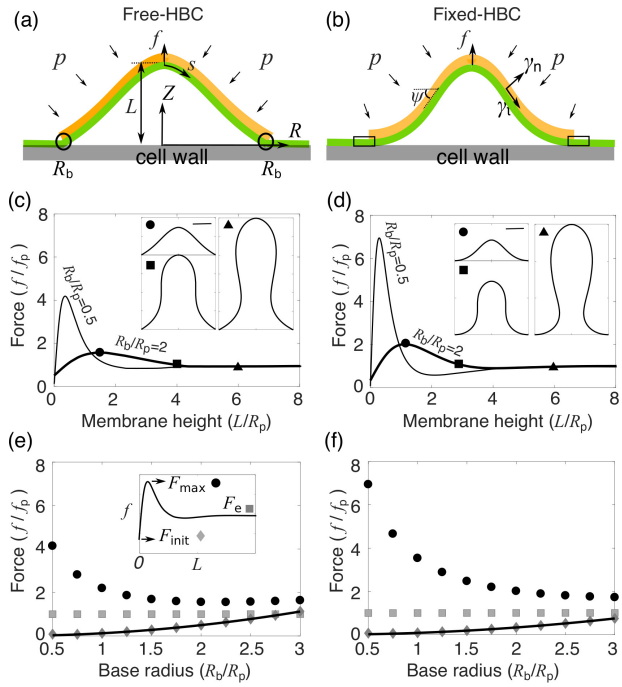

FIG. 1. (Color online) Effect of base radius on membrane deformation and force requirement. (a, b) Illustration of the model in which a membrane (green layer) is pulled up by a point force f against osmotic pressure p. The membrane is coated with proteins (orange layer) that produce spontaneous curvature c_0. Free-HBC is imposed at the attachment point $R = R_\mathrm{b}$ in (a), and fixed-HBC in (b). (c, d) Force-height (f-L) curves for different base radii R_b with free-HBC in (c) and fixed-HBC in (d). Insets show membrane shapes at the points indicated by symbols on the $f - L$ curve for $R_\mathrm{b} = 2R_\mathrm{p}$. The square indicates the critical shape where the membrane is about to form a neck. The scale bar is R_p. (e, f) The peak force F_max (circle), initiation force F_init (diamond) and elongation force F_e (square) for various R_b with free-HBC in (e) and fixed-HBC in (f). The solid curve represents the analytical solution for F_init.

independent of R_b [24]; (ii) When pressure dominates, the peak force F_{max} significantly varies with base radius R_b (Fig. 1e and f, solid circles), whereas in the tension-dominant regime, F_{max} always overshoots 13% relative to the equilibrium force f_σ [24], independent of R_b.

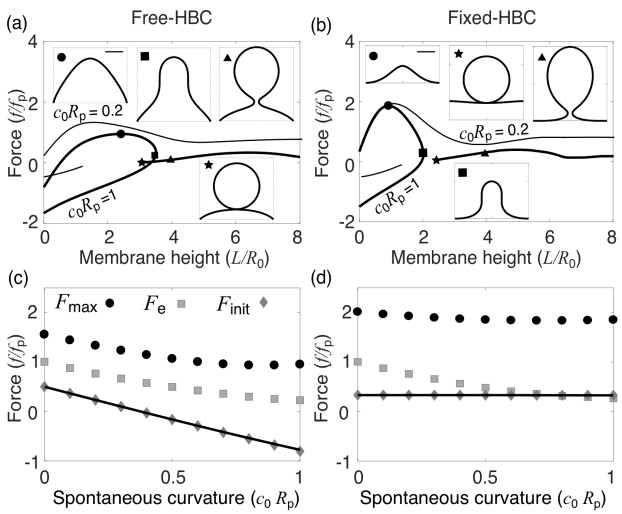

FIG. 2. Effect of spontaneous curvature c_0 on membrane deformation and force requirement. (a, b) The f-L curves for different c_0 with free-HBC in (a) and fixed-HBC in (b). Insets show membrane shapes at the points indicated by symbols on the f-L curve for $c_0R_p = 1$. The square indicates the critical shape where the membrane is about to form a neck. The scale bar is R_p. (c, d) The peak force F_{max} (circle), initiation force F_{init} (diamond) and elongation force F_e (square) for various c_0 with free-HBC in (c) and fixed-HBC in (d). The solid curve represents the analytical solution for F_{init}.

We then consider the effect of membrane curvature c_0 induced by proteins on membrane deformations. The base radius is fixed at $R_b = 2R_p$. For both boundary conditions, at large c_0, the f-L curve is broken into two branches, one with a low membrane height (small L), the other with a high membrane height (large L). In the small-L branch, one L has two corresponding forces f. The larger f corresponds to a solution with a dimple shape (Fig. 2a and b, inset, circles), while the smaller f corresponds to solution with an Ω-shape. The free energy of the dimple-shape is lower than the Ω-shape, therefore more stable [27]. The large-L branch starts from a point at which the force f is almost zero, and exhibits a vesicular shape budding off from the membrane (Fig. 2a and b, inset, pentagons). This implies that if a long tube is pulled out and maintained by a force, when the force is released, a vesicle will spontaneously form.

We also notice a qualitative difference in the f-L curve between the two boundary conditions. Under free-HBC, the initiation force F_{init} drops down with increasing c_0 and becomes even negative for $c_0R_p > 0.4$, which implies that the membrane patch can be lifted off the cell wall without external forces. By contrast, under fixed-HBC, the initiation F_{init} remains almost constant (Fig. 2 c and d, solid lines and diamonds). In addition, the force barrier F_{max} has a noticeable reduction with increasing c_0 under free-HBC, while F_{max} almost has no change under fixed-HBC (Fig. 2 c and d, solid circles). As for the elongation F_e, both boundary conditions give the same value, which is essentially the force obtained by approximating the membrane shape as a cylinder.

So far we have considered deformations of membrane with a homogenous spontaneous curvature c_0. This describes a membrane coated with proteins that produce membrane curvature c_0 and the coating area is growing with the patch. We next extend our model to the case where the coating area of curvature-producing proteins is constant. In this case, the spontaneous curvature is spatially varied as

$$c_0(a) = \frac{c_0}{2}\left\{1 - \tanh[\alpha(a - a_0)]\right\}, \tag{10}$$

where $a(s)$ is the surface area that obeys $\dot{a} = 2\pi R$. The coating area is a_0 and the parameter α controls the sharpness of the coating edge. The membrane tension σ for this inhomogeneous membrane is no longer a constant but spatially varies to enforce the area of membrane is locally unstretched [8], and is governed by

$$\dot{\sigma} = \kappa\left(\frac{\sin\psi}{R} + \dot{\psi} - c_0\right)\dot{c_0}. \tag{11}$$

We then consider the effect of coating area of proteins a_0 on the membrane deformation. The spontaneous curvature and the base radius are fixed at $c_0R_p = 1$ and $R_b = 2R_p$. Under both boundary conditions, for large a_0, instead of showing a single peak force F_{max} as seen on the f-L curve for small a_0, two local peak forces F^1_{max} and F^2_{max} are present (Fig. 3 a and b). The first peak F^1_{max} can be reduced to even below the elongation force $F_e = f_p$. The second peak F^2_{max} is slightly greater than f_p (Fig. 3 c and d, solid circles and pentagons). Under free-HBC, the initiation force F_{init} goes down and remains negative with increasing a_0. However, under fixed-HBC, F_{init} are positive for both small and large a_0, but are negative for intermediate values of a_0 (Fig. 3c and d, diamonds).

To test the validity of our theory, we compare the calculated membrane shapes with that obtained by electron microscopy in budding yeast (Fig. 4) [6]. Based on the observation that the coating area of clathrin remains constant during CME [7] and the number of clathrin molecules fits a hemispherical cap [28], we assume a coating area of proteins $a_0 = 2\pi R_p^2$ that induce a membrane curvature $c_0 = 1/R_p$. The characteristic radius R_p is chosen such that the membrane neck is absent until the membrane height reaches $L = 42$nm as observed experimentally. For free-HBC, one gets $R_p = 15$nm and for fixed-HBC $R_p = 18$nm. Here we show the results for

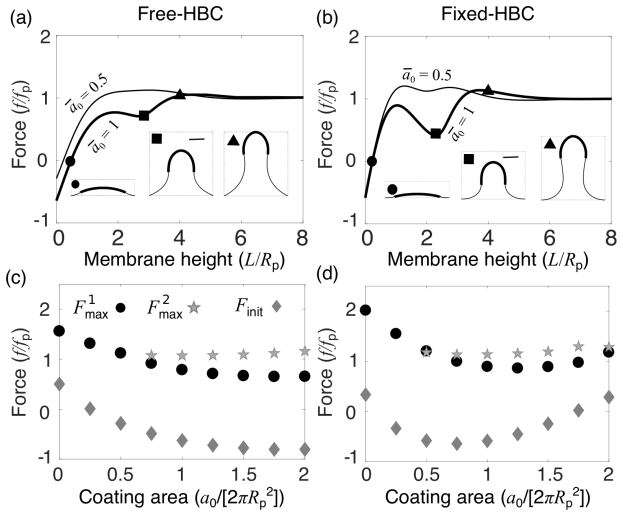

FIG. 3. Effect of coating area a_0 of curvature-generating proteins on membrane deformation and force requirement. (a, b) The f-L curves for different coating area a_0 with free-HBC in (a) and fixed-HBC in (b). Insets show membrane shapes at the points indicated by symbols on the f-L curve for $\bar{a}_0 \equiv a_0/(2\pi R_{\rm p}^2) = 1$. The square indicates the critical shape where the membrane is about to form a neck. The thick part represents the area coated with proteins. The scale bar is $R_{\rm p}$. (c, d) The first peak force $F^1_{\rm max}$ (circle), the second peak force $F^2_{\rm max}$ (pentagon) and the initiation force $F_{\rm init}$ (diamond) for various a_0 with free-HBC in (c) and fixed-HBC in (d).

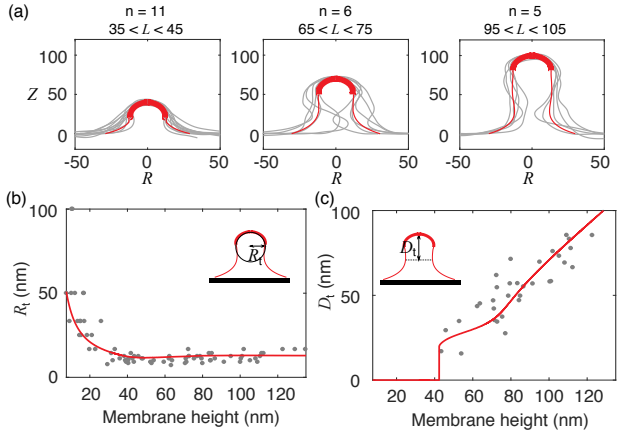

FIG. 4. (Color online) Comparison with experimental results. (a) Membrane shapes obtained by electron tomography are grouped according to heights and overlaid at the tip [6]. The calculated membrane shapes with free-HBC are represented by the red curves, with the thick part indicating the coating area of proteins. The unit is nm. (b, c) Comparison of two geometric features of $R_{\rm t}$ and $D_{\rm t}$ between theory (line) and experiments (dots). Parameters are $p = 1{\rm MPa}, R_{\rm p} = 15{\rm nm}, c_0 = 1/15{\rm nm}^{-1}, a_0 = 1414{\rm nm}^2, \alpha = 10/(2\pi R_{\rm p}^2), \sigma = 0.03{\rm pN/nm}$.

free-HBC and leave the results for fixed-HBC in the supplement. The experimental shapes are divided into three groups to represent different stages of endocytosis according to the membrane height. Our calculated shapes agree well with the experimental data, particularly in the early stage when the membrane height is low (Fig. 4 a). For membrane shapes that are higher than 65nm, experimental membrane shapes are typically asymmetric and exhibit a narrower neck than the calculated ones, probably due to the presence of other membrane proteins that arrive later during endocytosis and that produce large curvatures at the neck of the invagination.

We also compare two geometric features of the membrane shape calculated by our theory with experimental data. One is the tip radius $R_{\rm t}$ which is the reciprocal of the mean curvature $\dot{\psi}$ averaged over an arc that extends over 15nm from the tip of the invagination [6] (Fig. 4 b). The other is the distance between the neck and the tip $D_{\rm t}$ (Fig. 4 c). The tip radius $R_{\rm t}$ drops from 50nm to 13nm as the membrane height increases, and our theory fits well with the experimental data (Fig. 4 b). When necks appear, the distance from neck to tip $D_{\rm t}$ initially grows slowly with membrane height. When $L > 80$nm, D_t scales almost linearly with L (Fig. 4 c) with a larger slope than the initial phase, again matching well with the experimental data.

Our results suggest that boundary conditions at the points where the membrane is attached to the cell wall can generate qualitatively different results for the force requirement of membrane deformation. This helps explain the results discovered in Ref. [10] that induced membrane curvature by proteins hinders CME by increasing the initiation force $F_{\rm init}$. The authors adopted a similar model to our homogeneous membrane but a slightly different fixed-HBC than ours. Instead of fixing the base radius $R_{\rm b}$, they require the conjugate variable of $R_{\rm b}$, the tangential tension $\gamma_t = 0$ and arrived at the conclusion $F_{\rm init} \propto c_0$. In that case, a large external torque τ, which is proportional to c_0, has to be applied to enforce the angle $\psi = 0$ at the contact point, and the large initiation force might be a result of the large external torque.

The comparisons with experiments for partially coated membrane suggest that proteins that induce membrane curvature, such as clathrin, indeed facilitate CME, regardless of the boundary conditions. A shallow dimple-shaped membrane invagination can be spontaneously formed without any forces. With the fitting parameter $R_{\rm b}$ obtained to match the membrane height at which a neck appears, we infer that the force barrier for CME in yeast can be reduced to ~ 2000pN for free-HBC and ~ 3000pN for fixed-HBC with the assistance of a clathrin coat. However, this is still beyond the force that can be generated by polymerization of $150 - 200$ actin filaments at the endocytic site [28]. Investigating non-polymerization based force production by actin machin-

ery will be our future work. A possible way is to release the elastic energy stored in geometrically frustrated crosslinkers, such as fimbrin [29].

This research is supported by National Institutes of Health/National Institute of General Medical Sciences Grant R01GM115636.

* ruima86@gmail.com
† julien.berro@yale.edu

[1] M. Kaksonen and A. Roux, Nature Reviews Molecular Cell Biology **19**, 313 EP (2018).
[2] M. M. Lacy, R. Ma, N. G. Ravindra, and J. Berro, FEBS Letters **0** (2018), 10.1002/1873-3468.13192.
[3] R. Basu, E. L. Munteanu, and F. Chang, Molecular biology of the cell **25**, 679 (2014).
[4] N. Minc, A. Boudaoud, and F. Chang, Current Biology **19**, 1096 (2009).
[5] E. Atilgan, V. Magidson, A. Khodjakov, and F. Chang, *Current Biology*, Current Biology **25**, 2150 (2015).
[6] W. Kukulski, M. Schorb, M. Kaksonen, and J. A. Briggs, Cell **150**, 508 (2012).
[7] O. Avinoam, M. Schorb, C. J. Beese, J. A. G. Briggs, and M. Kaksonen, Science **348**, 1369 (2015).
[8] A. Agrawal and D. J. Steigmann, Biomechanics and Modeling in Mechanobiology **8**, 371 (2008).
[9] N. Walani, J. Torres, and A. Agrawal, Proceedings of the National Academy of Sciences **112**, E1423 (2015).
[10] S. Dmitrieff and F. Nédélec, PLoS Comput Biol **11**, 1 (2015).
[11] J. E. Hassinger, G. Oster, D. G. Drubin, and P. Rangamani, Proceedings of the National Academy of Sciences **114**, E1118 (2017).
[12] G. Koster, A. Cacciuto, I. Derényi, D. Frenkel, and M. Dogterom, Phys. Rev. Lett. **94**, 068101 (2005).
[13] D. Cuvelier, I. Derényi, P. Bassereau, and P. Nassoy, Biophysical Journal **88**, 2714 (2005).
[14] R. Dimova, S. Aranda, N. Bezlyepkina, V. Nikolov, K. A. Riske, and R. Lipowsky, Journal of Physics: Condensed Matter **18**, S1151 (2006).
[15] A. E. Carlsson, Current Opinion in Cell Biology **50**, 1 (2018), cell Architecture.
[16] A. E. Carlsson and P. V. Bayly, Biophysical Journal **106**, 1596 (2014).
[17] X. Wang, B. J. Galletta, J. A. Cooper, and A. E. Carlsson, Biophysical Journal **110**, 1430 (2016).
[18] D. J. Tweten, P. V. Bayly, and A. E. Carlsson, Phys. Rev. E **95**, 052414 (2017).
[19] M. Mund, J. A. van der Beek, J. Deschamps, S. Dmitrieff, P. Hoess, J. L. Monster, A. Picco, F. Nédélec, M. Kaksonen, and J. Ries, Cell **174**, 884 (2018).
[20] T. Kirchhausen and S. C. Harrison, Cell **23**, 755 (1981).
[21] A. Fotin, Y. Cheng, P. Sliz, N. Grigorieff, S. C. Harrison, T. Kirchhausen, and T. Walz, Nature **432**, 573 EP (2004).
[22] W. Helfrich, Zeitschrift für Naturforschung C **28**, 693 (1973).
[23] M. Deserno, Chemistry and Physics of Lipids **185**, 11 (2015), membrane mechanochemistry: From the molecular to the cellular scale.
[24] I. Derényi, F. Jülicher, and J. Prost, Phys. Rev. Lett. **88**, 238101 (2002).
[25] A. J. Jin, K. Prasad, P. D. Smith, E. M. Lafer, and R. Nossal, Biophysical Journal **90**, 3333 (2006).
[26] See Supplemental Material at [URL] for detailed description of the numerical methods to obtain the force-height curve, and derivations of the analytical solution to the initiation force F_{init}.
[27] See Supplemental Material at [URL] for the free energy and the Ω-shape, which in some cases have certain part of the membrane below the cell wall.
[28] V. Sirotkin, J. Berro, K. Macmillan, L. Zhao, T. D. Pollard, and S. L. Schmid, Molecular Biology of the Cell **21**, 2894 (2010), pMID: 20587778.
[29] R. Ma and J. Berro, PLOS Computational Biology **14**, 1 (2018).